Room Temperature Crossbar H-typer Cavity Testing and Conditioning

Jose´ Gallegos
Community College Institute of Science and Technology

College of DuPage, Glen Ellyn, IL

Supervised by:
David Wildman/Robyn Madrak

Fermi National Accelerator Laboratory
Batavia, Illinois

May 23 - August 19, 2011

Abstract

Fermilab's High Intensity Neutrino Source (HINS) Linac consists of a normal-conducting and a superconducting section. The normal-conducting section is comprised of 16 room temperature crossbar H-type (RT-CH) 325 MHz cavities, which will take the beam energy from 2.5 MeV to 10 MeV. To obtain optimal performance, the 16 cavities need to be conditioned and tested before being installed. This paper will give a description of the normal-conducting cavities and will also describe the process used in conditioning the cavities.

Introduction

The High Intensity Neutrino Source (HINS) is an R&D facility aimed at demonstrating the feasibility of an 8 GeV superconducting H-Linac. The 8 GeV Linac would replace Fermilab's existing injector complex with an intended beam power of 2 MW, enabling Fermilab to support future programs that demand high intensity proton beam.

The HINS Linac is comprised of a 50 keV H- ion source that provides beam to a 2.5 MeV radio frequency quadrupole (RFQ). The RFQ is followed by a medium energy beam transport section and up to a total of 16 room temperature crossbar H-type (RT-CH) cavities which take the beam energy from 2.5 MeV to 10 MeV. If installed, two cryomodules would house 16 superconducting (SC) single-spoke cavities that will bring the beam energy to 30 MeV. The final 30 MeV would be achieved by one cryomodule housing 11 SC spoke cavities, which would bring the final energy to 60-65 MeV [1].

The HINS Linac would be the first low-energy, high-intensity proton/H- linear accelerator to incorporate superconducting solenoids for transverse focusing, high power RF vector modulators for independent control of multiple cavities powered by one kystron, and superconducting spoke-type accelerating cavities starting at 10 MeV [2].

Thus far, the RFQ has been tested and ran successfully, next in line is the warm section of HINS Linac. Coming into to this internship, six RT-CH cavities were already tested and conditioned and were ready to be installed in the beam line. The remaining cavities still needed to be conditioned and tested. The testing and the conditioning process will be described in this paper.

Cavity Description

The room temperature crossbar H-type cavity is a 325 MHz half wavelength resonator. The main body is a 10 mm thick cylinder made of oxygen free electronic copper (Cu-OFE) with an internal diameter of 364 mm and a varying length depending on its position along the beam line. Since the cavity is under vacuum, the ends are designed to assure structural integrity with an outer 5 mm stainless steel plate. An inner 3 mm Cu-OFE plate is used for RF (high Conductivity), with a 2 mm air gap in between the cooper and stainless steel [2]. The cavities are designed with either three spokes and four accelerating gaps or four spokes and five accelerating gaps, depending on their position along the beam line. The electric field is not the same in each gap. The magnitude in the first and last gaps is half of that in the center gaps. For example, RT-CH 3 has four gaps and a total integrated gap voltage of 0.33 MV with 55 KV on the end gaps and 111 KV in the center gaps. The RF input coupler is a copper loop which drives the cavity at its resonant frequency. It is designed with Ansoft high frequency structure simulator software, and it is used for all 16 cavities. A plunger-type tuner is used to control the resonant frequency and is capable of a tuning range of ± 0.3 MHz.

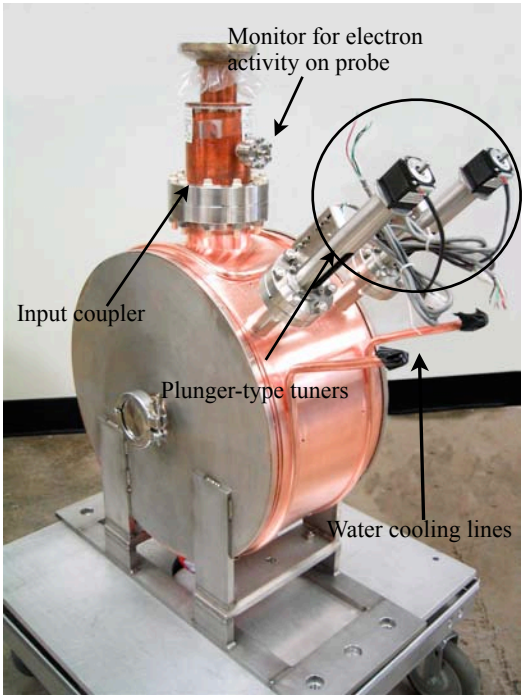

Figure 1: The first cavity designed RT-CH 1. Note: originally designed with two tuner, now there will only be one.

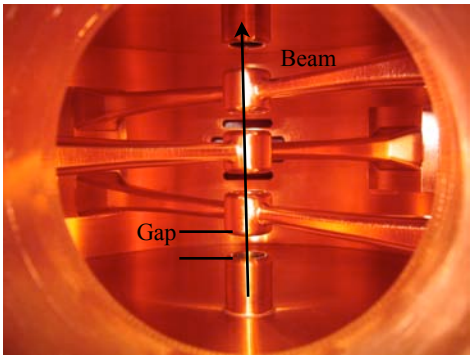

Figure 2: The interior of the RT-CH 1 as seen from the input coupler port showing the beam path.

The original plan was to use 16 unique cavity designs (the first four as 4-gap cavities and remaining twelve as 5-gap cavities). Each cavity was optimized with a corresponding geometrical beta ($\beta = v/c$) ranging from $\beta = 0.0744$ to 0.1422, which would take the beam energy from 2.5 MeV to 10 MeV. However, after the first four were built, it was decided to use fewer designs with the remaining twelve to save on cost and time. Now, there are a total of nine unique designs. Table 1 shows the key design parameters for all cavities. After the first four, there are 2-3 identical cavities in each of the five groups. Due to this small reduction in the efficiency of acceleration, the power loss is increased from 348.8 KW to 353.2 KW.

Beta	Voltage (MV)	Cavity number	R_{sh} (MΩ)	P_{copper} Loss (KW)	Cavity Design #	R_{sh} (MΩ)	New P_{copper} Loss (KW)
0.0744	0.1439	1	10.392	1.9912	1	10.392	1.9912
0.0771	0.2489	2	10.9	5.6814	2	10.9	5.6814
0.0804	0.3294	3	11.3	9.6025	3	11.3	9.6025
0.0842	0.3867	4	11.584	12.91	4	11.584	12.91
0.0882	0.4795	5	17.234	13.339	5	17.234	13.339
0.0923	0.5061	6	18.04	14.197	5	17.224	14.87
0.0968	0.5743	7	18.82	17.527	8	18.392	17.934
0.1015	0.6143	8	19.532	19.322	8	19.532	19.322
0.1063	0.7297	9	20.24	26.305	8	19.514	27.284
0.1111	0.7051	10	20.9	23.791	11	20.608	24.128
0.1159	0.7387	11	21.474	25.41	11	21.474	25.41
0.121	0.8016	12	22.08	29.098	11	21.308	30.152
0.1262	0.8619	13	22.62	32.843	14	22.286	33.335
0.1316	0.9182	14	23.168	36.39	14	23.168	36.39
0.1371	0.9882	15	23.58	41.416	16	23.342	41.838
0.1422	0.9671	16	23.954	39.047	16	23.954	39.047

Table 1: New plan design parameters for all cavities.

The Pumpdown process

The cavities were put under ultrahigh vacuum in order to conduct our tests. In the pumpdown process, three different pumps were used in order to achieve a vacuum of ~1x10^-8 torr. The first pump used was the roughing pump, which operates in the range of 760 torr to 1x10^-3 torr. The turbomolecular pump, the second pump used, operates in the range of 1x10^-3 torr to 1x10^-8 torr. The ion pump was the final pump used, which operates at the range of

1x10^-8 torr and below [3]. The pumpdown process was monitored in order to check for leaks. However, a perfect vacuum can never be achieved due to outgassing, which will be discussed in this report. Virtual leaks and real leaks can be distinguished in a pumpdown graph of system pressure against time. With a real leak, the system reaches a point where the leak is providing the same amount of air as is being pumped out, and therefore the graph becomes flat. Virtual leaks are trapped volumes that release gases very slowly into the system, they shift the curve from a normal pumpdown curve but the pressure continues to decrease. During the pumpdown of RT-CH 6, 10, and 7 there were no real leaks observed. This was determined since the graph followed a normal pumpdown curve of a -1 slope on a log-log graph, as shown in figure 3.

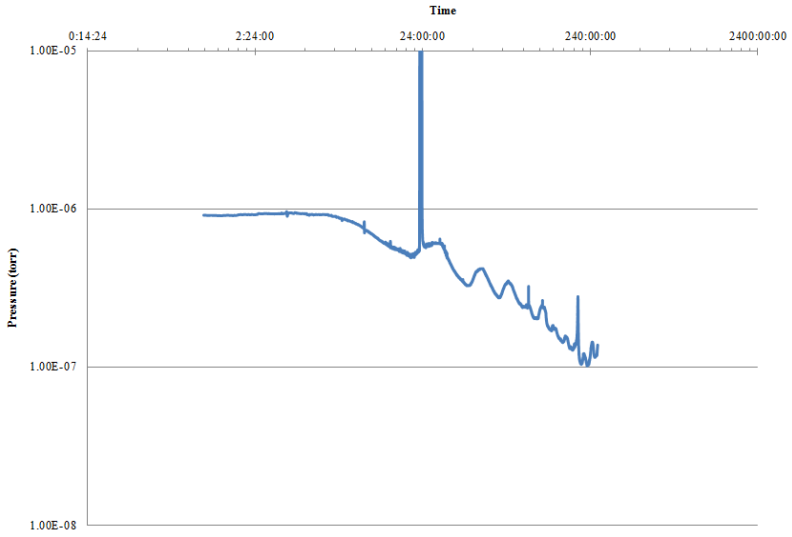

Figure 3: A log-log graph of pressure against time for RT-CH 6

Testing the Cavity

One of the main reasons for conducting the test was to condition the cavity. In order to do this, the cavity had to be under vacuum and inside a cavity test cave for X-ray radiation shielding purposes. The RF power is supplied by a 325 MHz 2.5 MW Toshiba E3740A klystron. Cleaning of the interior is achieved by electron bombardment, which is known as multipactoring. When an oscillating potential is applied between two surfaces, in a vacuum; and if the voltage, frequency, and spacing are such that the time of flight of an electron between the surfaces is an odd multiple

of a half period of the oscillation, electron multiplication by secondary emission may occur [4]. The threshold voltage is given in equation 1 where m is the mass of an electron, e is the charge of an electron, ω is 2πf, and n is the order of multipactoring. Equation 1 can be simplified to the first order of multipactoring as shown with equation 2, where f is the frequency in MHz and d is the spacing in inches.

$$V_t = \frac{m/2e\,(\omega d)^2}{\sqrt{\{1+[(2n-1)\tfrac{1}{2}\pi]^2\}}} \qquad (1) \qquad\qquad V_t = 0.039(fd)^2 \qquad (2)$$

Multipactoring was first observed in RT-CH 6 at a forward power of 350 watts with a reflected power of 100 watts at a frequency of 325.036 MHz. With a total accelerating gap voltage of 0.47 MV, ohmic losses (Pc) are 12.1 KW. The total gap voltage is distributed among the five accelerating gaps, as discussed earlier: (60 KV, 120 KV, 120 KV, 120 KV, 60 KV). Knowing this, one can predict the location of multipactoring in RT-CH 6 at a forward power of 350 watts. Since $P_c \approx P_f - P_r = 250$ watts, and $P = V^2/R$, the total gap voltage at 250 watts can be calculated as:

$$\sqrt{(250\text{ W}/12.1\text{ KW})} \times 0.47\text{ MV} = 67.56\text{ KV}$$

Therefore, we know the voltage distribution was (8.44KV, 16.89 KV, 16.89 KV, 16.89 KV, 8.44 KV). Figure 4 shows a graph of multipactoring threshold voltage with respect to distance at a frequency of 325.036 MHz, and it shows that multipactoring took place between the spokes and the walls of the cavity approximately at a distance of 1.43 inches from the end wall and the first spoke or 2.02 inches between the spokes. Figure 5 shows possible multipactoring locations.

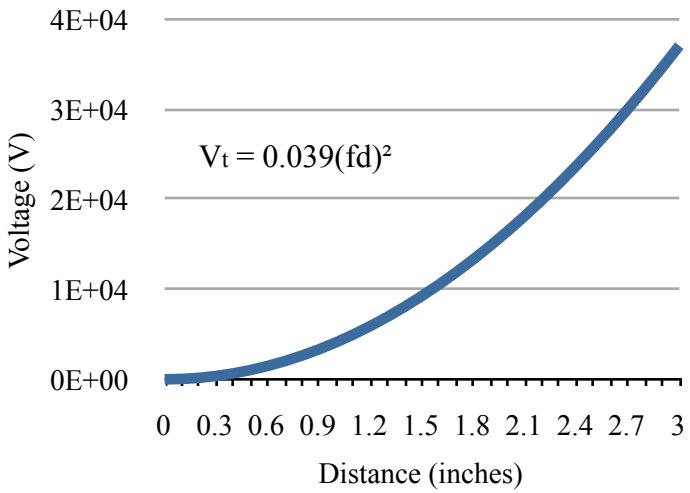

Figure 4: A plot of threshold voltage against distance in inches with a corresponding frequency of 325.036 MHz.

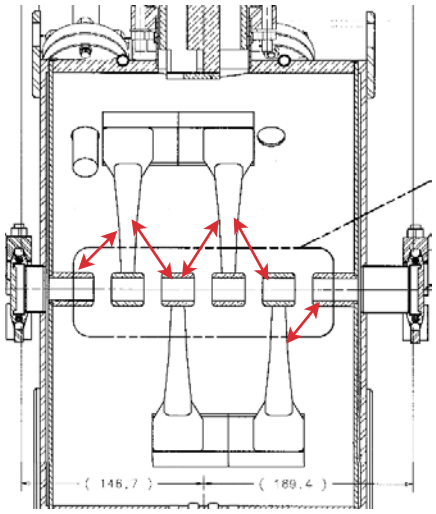

Figure 5: A drawing of the interior of RT-CH 6 with possible multipactoring locations.

Figures 6 and 7 show a cavity's electric field (pink), forward power (yellow), and the reflected power (blue). When there is no multipactoring, the electric field increases and decreases exponentially at the beginning and end of every pulse as shown in figure 6. However, during multipactoring the electric field is decreased by the multipactoring electrons, as shown in figure 7. The reflected power is also affected. In the absence of multipactoring reflected power will have two sharp peaks at the beginning and end of each pulse. During multipactoring, the exchange of electrons

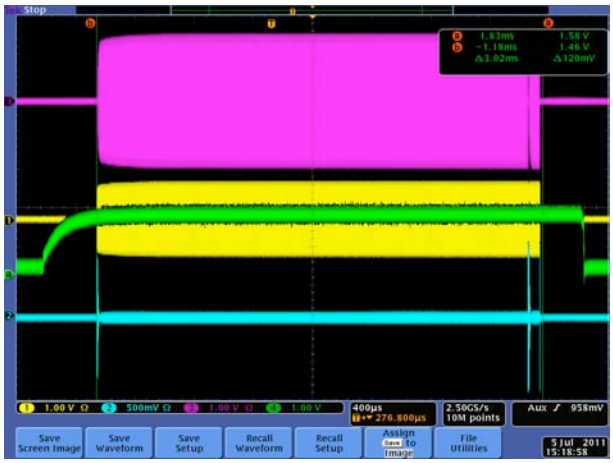

Figure 6: The pulse in a multipactoring-free cavity.

between two surfaces changes the impedance of the cavity and the coupling loop system, this will change the shape of the reflected power pulse. Equation 3 shows the relationship between the impedance of the transmission line (Z_1) and the coupling loop and cavity impedance (Z_2). As the cavity and coupling loop impedance change, The reflected power does also.

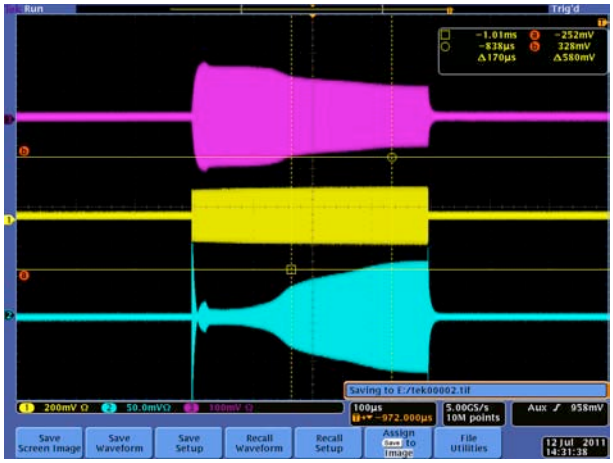

Figure 7: The pulse in a multipactoring cavity.

$$P_r = P_f \left[\frac{Z_2 - Z_1}{Z_2 + Z_1} \right]^2 \qquad (3)$$

The exchange of the electrons between two surfaces can be modeled as a capacitor discharging, and therefore decreasing in voltage. The upper multipactoring voltage limit (V_{uM}) is reached when the current of the second electron emission (I_2) is sufficient enough to drop the voltage of the modeled capacitor plates below its threshold multipactoring voltage [4].

$$V_{um} < 1.85V_t \qquad (4)$$

In order for that to happen, the coefficient of secondary electron emission ($\sigma = I_2/I_1$), where I_1 is the primary electron current, needs to be greater than one. When $\sigma > 1$, cavity voltage (U_c) will drop exponentially and reflected power will grow in the same manner (since I_2 is causing the voltage to drop). The voltage will drop below the threshold voltage, and multipactoring will stop. At this time, the cavity will begin to fill at a constant rate, depending on the Q of the the cavity, and reflected power will decrease at the same rate. The increase in voltage will, again, cause

multipactoring to begin and reach σ > 1 and the process will continue for each pulse. Figure 8 shows the modulation in reflected power due to multipactoring.

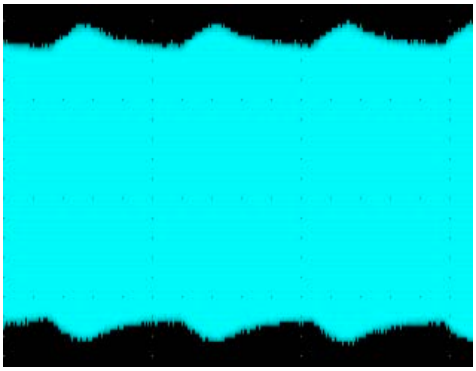

Figure 8: The modulations of the reflected power caused by multipactoring.

In order to complete our test, the cavities had to be driven at or above 125% of the intended power loss. Initially, the cavities were driven at their resonant frequency at a low power (~200 W), a small pulse length (~0.1 ms), and at a pulse frequency of 1 Hz. The power and pulse length were increased incrementally until reaching the desired power. As these parameters were increased, multipactoring diminished and contaminants were pumped out. As the pulse length and the frequency were increased, the resonant frequency had to be adjusted to account for cavity expansion due to heating. Table 2 show the final conditions of three cavities that were completed.

Cavity	Resonant frequency	Final forward power	Final pulse length	Final pulse Frequency	Time to complete test
RT-CH 6	325.065 MHz	27.4 KW	3 ms	2 Hz	19 hrs
RT-CH 10	324.98 MHz	30.6 KW	3 ms	2 Hz	27 hrs
RT-CH 7	325.018 MHz	31.52	3 ms	2 Hz	18 hrs

Table 2: Final testing conditions of the three cavities that were completed.

Outgassing

During multipactoring, at the threshold voltage, electrons are released from the surface. The bombardment by free electrons of the interior of the cavity, releases contaminants from the

copper surface in a process know as outgassing. As these contaminants are released the pressure rises. Outgassing also occurs due to thermal energy. By valving out the turbo pump and shutting down the ion pump, we were able to measure the thermal outgassing rate of RT-CH 7, determined to be 8.874x10^-7 torr l/s (torr-liters per second), at room temperature. The pressure (P) was also measured to be 3.77x10-7 torr, with only the ion pump running. Since outgassing rate = PS, where S is the pumping speed, the pumping speed of the ion pump was determined to be 2.35 l/s. The ion pump has a specified pumping speed of 30 l/s. The drop in pumping speed is due to the ion pump being limited by the conductance (C) of the pipes used. Conductance depends on the diameter (D) and the length (L) of the pipes in inches, as shown in equation 5.

$$C = \frac{75D^3}{L} \qquad (5)$$

Using a diameter of 1.5 inches, our calculations show that the length of the pipe is 107.71 inches, which is notably larger than the actual length. This inconsistency could be due to the 90 degree elbows or the temperature difference between the time the outgassing rate was measured compare to when the pressure was measured.

Q and β Measurements

During cavity testing, other measurements were performed. The cavity was driven at its fundamental resonant frequency. For each pulse, the total power loss is the sum of the power dissipated in the cavity's walls (ohmic losses) and the the power that leaks out of each coupler. P_e is the power leaking back out of the input coupler, and P_t is the power leaking from the transmitted power coupler.

$$P_{tot} = P_c + P_e + P_t \quad (6)$$

The transmitted power probe is coupled to the cavity very weakly, which minimizes its effects on our measurements, and therefore it will be neglected. The unloaded quality factor (Q_o), the loaded quality factor (Q_L), and the external quality factor (Q_e) are defined as, where U is the stored energy. [5]

$$Q_o = \frac{\omega U}{P_c} \quad (7) \qquad Q_L = \frac{\omega U}{P_{tot}} \quad (8) \qquad Q_e = \frac{\omega U}{P_e} \quad (9)$$

The coupling strength (β) (different from the previous β = v/c) determines how strongly the couplers interact with the cavity. Expressions are given in equation 10. Equation 11 can be derived by solving for P_{tot}, P_e, and P_c in equations 7, 8, and 9, substituting them into equation 6, and factoring out a $1/Q_o$ from the right side.

$$\beta = \frac{Q_o}{Q_e} = \frac{P_e}{P_c} \quad (10) \qquad \frac{1}{Q_L} = \frac{1}{Q_o}(1 + \beta) \quad (11)$$

If β > 1 (overcoupled), it implies that the amount of power leaking from the coupler is large compared to ohmic losses, and if β < 1 (undercoupled), the opposite is true [5]. The optimal condition with beam is if β = 1, so there is minimum power reflected. Since during beam loading additional losses are introduced, the cavity needs to be overcoupled during cavity testing (without the beam). β can be expressed as equation 12, where P_b is beam power loss.

$$\beta = \frac{P_e}{P_c + P_b} \quad (12)$$

Setting equation 12 equal to one, we arrive at equation 13.

$$1 = \frac{P_e / P_c}{1 + (P_b / P_c)} \qquad (13)$$

Cavity RT-CH 10 was measured to have a Q_o of 11980 and $Q_L = 4870$. With equation 11, we see that $\beta = 1.46$. Therefore P_b/P_c needs to be equal to 0.46, to achieve the matched condition with beam.

Phase Measurements

During particle acceleration, the particle beam needs to be in phase with the electric field in the cavities. If a particle arrives in the cavity when the electric field is in the "wrong" direction, it will be decelerated. A particle with synchronous phase corresponds to the perfect particle, having the perfect energy, arriving in the cavity at the desired time, when the electric field is at its desired value, as shown at point S in figure 10. Those particles that arrive too early are given less energy, which correspond point E, and those particles that arrive too late are given more energy than normal, which correspond to point L. To phase the beam correctly with respect to the cavity, it is necessary to measure the cavity phase with respect to the RF drive.

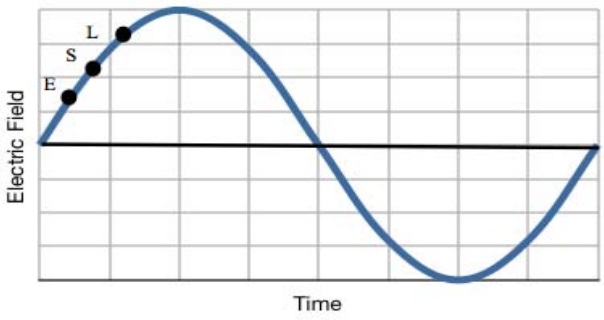

Figure 9: An electric field showing the possible particle arrive point.

A network analyzer was used to measure this precisely. A S21 thru calibration was first performed in order to correct for the length of the cables attached to the network analyzer. Various adaptors were also used to connect the cables during calibration and cavity phase measurements, which also must be taken into consideration. Therefore, three adapters were also measured in order to find the true phase difference. The three

adapters measured are shown in table 3. In order to calibrate the cables, the N-type female to SMA female adaptor was used, then removed for the measurement, and the N-type to 1 5/8 adapter was installed on the cavity. Therefore, to obtain the correct phase, 11.5364° (N-type female to SMA female adapter's phase difference) was subtracted from the measured phase and 42.794° (N-type to 1 5/8 adaptor's phase difference) was added, which gave us the true phase difference for each cavity. Since the bunchers have a different connector on the transmitting port, a N-type bullet was used in place of the N-type female to SMA female adaptor.

S11 measurements were also conducted for future inquires. The phase offset is the reading on the network analyzer after the calibrations were performed and before the cavity was connected. Measurements were corrected for the phase offset and converted to a positive value. The phase difference due to the 1 5/8 adaptor was subtracted twice, since the wave travels down and back in an S11 measurement. The results are shown in table 3.

Adaptor:	N-type Bullet		N-type to SMA (female-female) Adaptor		N-type to 1 5/8 Adaptor		
Phase measurement: (degrees)	14.708		11.5364		42.794		
FP CAVITY CALIBRATIONS							
	S21 Measurements						
	Resonant Frequency (MHz)	Power (dB)	Quality Factor	Measured phase (degrees)	True Phase (degrees)		
Cavity 1	324.84021	-31.14	5000	-42.676	-11.4184		
Cavity 2	324.96529	-35.3	3955	-18.5	12.7576		
Cavity 3	325.18168	-36.35	4045	-19.65	11.6076		
Cavity 4	325.22796	-37.35	4355	-17.15	14.1076		
Cavity 5	325.12477	-35.81	4475	-12	19.2576		
Cavity 9	325.24609	-39.3	4720	-10.77	20.4876		
Buncher 1	325.05097	-29.72	11108	-20.9	10.3576		
Buncher 2	325.03221	-37.08	11520	-11.6	19.6576		
	S11 Measurements						
	Resonant Frequency (MHz)	Power (dB)	Phase offset (degrees)	Phase (degrees)	measured phase minus offset	correct to positive	True Phase (degrees) *
Cavity 1	324.8596	-18.03	-1.14	-154.6	-153.46	153.46	67.872
Cavity 2	324.96842	-15.45	-1.31	25.5	26.81	333.19	247.602
Cavity 3	325.1848	-16.65	-0.93	18	18.93	341.07	255.482
Cavity 4	325.22983	-19	-0.8	23	23.8	336.2	250.612
Cavity 5	325.12602	-15.85	-1.31	21	22.31	337.69	252.102
Cavity 9	325.24734	-15.377	-1.35	18.5	19.85	340.15	254.562
Buncher 1	325.0541	-30	-1.55	22.2	23.75	336.25	250.662
Buncher 2	325.03408	-24.1	-1.55	18.9	20.45	339.55	253.962
*Note:	The N to 1 5/8 adapter phase difference was subtracted twice from the phase measured in S11.						

Table 3: S21 and S11 phase measurements of 6 cavities, and phase measurements of adaptor used.

Conclusion/Discussion

There are a total of eight cavities that have been conditioned, three of which I was involved in, and one that is in the process of being conditioned while this paper was being written (CH-RT 12). The HINS project is, however, being cut back in favor of a continuous wave (as apposed to pulsed) accelerator. However, there are many aspects of this accelerator in which Fermilab is still interested, and therefore the project will continue. The remaining seven cavities will be conditioned and tested in the same manner as described here.

Acknowledgements

I want to take the opportunity to thank all of those who made this experience possible. I thank my mentors Dave Wildman and Robyn Madrak for their patience and guidance while working on my projects and writing this paper. Also, I would like to thank the CCI community for allowing me the opportunity to work at this prestigious laboratory. I acknowledge my instructors at College of DuPage for their guidance. And of course, I wouldn't have been able to do it without the support of my family and friends.

References

[1] R. C. Weber et al., “Overview of the High Intensity Neutrino Source Linac R&D Program at Fermilab”, Fermilab, Batavia, Illinois, USA, 2008.

[2] L. Ristori et al., “Fabrication and Test of the First Normal-Conducting Crossbar H-Type Accelerating Cavity at Fermilab for HINS”, PAC’07, Albuquerque, New Mexico, USA, WEPMN110, 2007

[3] Varian Associates Inc., Basic Vacuum Practice, 1992, Third Edition, Lexington, MA.

[4] B.H. Smith, “Radiofrequency systems of the Berkeley 88-inch Cyclotron,” Nuclear Instruments and Methods, Vol. 18, 1962, p. 184-193

[5] H. Padamsee et al., RF Superconducting for Accelerators, Cornell University, Ithaca, New york, Wiley-Interscience, 1998.